Full-wave analysis of the scattering of a pulsed light beam by dielectric cylinders embedded in a homogeneous medium

C. Ponti[1,2], M. Santarsiero[1], G. Schettini[1,2]

[1] Department of Engineering, Roma Tre University, via Vito Volterra 62, 00146 Roma, Italy

[2] National Interuniversity Consortium for Telecommunications, Roma Tre University, 00146 Roma, Italy

E-mail: `cristina.ponti@uniroma3.it`

January 2019

Abstract. An approach to study the time-domain scattering by a set of dielectric cylinders with circular cross section, placed in a semi-infinite medium, is presented. The illuminating light comes from a pulsed beam impinging onto the cylinders from outside the medium. The solution is developed in a semi-analytical way, starting from results based on the Cylindrical Wave Approach pertinent to the case of illumination by a monochromatic plane wave. The method is numerically implemented to simulate the scattering response of buried cylinders illuminated by a pulsed Gaussian beam. In the presented results, the different contributions to the total scattered field are recognizable, giving account of all the interactions between incident field, target and interface. The model adopted is well suited to the study, at optical frequencies, of scattering problems involving biological samples, such as vessels and fibers, embedded in tissues or immersed in fluids, through fast and accurate electromagnetic simulation.

1. Introduction

In several cases of notable interest in the optical domain, the capability of an accurate modelling of scattering by cylindrical dielectric objects is a tool that can give important support to the understanding of the behaviour of a phenomenon or the clarification of the internal structure of a complex system. Scattering by cylinders has in fact applications in the analysis of radiative properties and radiation energy transport through fiber materials [1, 2]. In the time-domain diagnostics through pulsed sources, the time-of-flight information in the scattered field allows to determine the internal structure of the tissue. In the field of OCT imaging, many approaches have been proposed.[3]-[9]. In [6], a Monte Carlo model is applied to the angiographic OCT imaging of small vessels in microvascular networks. However, radiative transfer is an approximate model, which neglects mutual interactions between the scatterers. Numerical full-wave models have been implemented in [7, 8] to simulate image formation in OCT for general samples.

An analytical solution for OCT applications is given in [9] for the case of a cylinder in free space, and time-domain analyses are proposed for plane-wave and Gaussian beam sources.

The extension of such techniques to cases where the cylindrical targets are embedded in a semi-infinite medium and the source field is of a different type represents a significant improvement. Several methods, both analytical and numerical [10]-[22], have been proposed in the literature to solve the scattering by objects in a semi-infinite medium in the frequency-domain. The time-domain response of the scattering by buried cylinders has received attention mainly at the microwave frequencies, due to the applications to remote sensing with the Ground Penetrating Radar [23, 24], or to breast cancer imaging [25].

A frequency-domain technique, developed for the simulation of two-dimensional scattering by buried objects, perfectly conducting either dielectric, is the Cylindrical Wave Approach (CWA) [16]. To deal with the field scattered by the buried cylinders, suitable reflected and transmitted cylindrical functions have been introduced as basis functions [34, 35]. The method has been implemented in the frequency domain to solve several scattering geometries, i.e., objects buried in a semi-infinite medium [16], embedded or buried below a dielectric layer [27]-[29], or under a rough surface [30]. In [31] it has been extended to solve the scattering of a pulsed plane-wave by conducting cylinders in a semi-infinite medium, in order to study typical waveforms used at the microwave frequencies in Ground Penetrating Radar technique.

In this paper, the theory for scattering of a monochromatic plane-wave by buried cylinders through the CWA is generalized to a pulsed field non uniform in time and space as the source of the scattering problem. Numerical results are given for a typical optical waveform as A-scan radargrams (one-dimensional plots of the scattered field at a fixed point as a function of time), or in the form of B-scans (two-dimensional maps obtained from a scanning of the scattered field along a line). Electric properties of biological tissues at optical frequencies have been considered in the simulations [36, 37] and an accurate evaluation of the scattered optical beam is carried out in this framework.

2. Theoretical Approach

2.1. Scattering of a monochromatic plane wave

In the present section we recall the results pertinent to the scattering of a monochromatic plane wave by a set of N cylinders, according to the CWA. The plane wave impinges onto the planar interface between two different linear, isotropic, homogeneous, dielectric and lossless semi-infinite media (from medium 0 to medium 1), as shown in Fig. 1. Refractive indices of the two media will be denoted by n_0 and n_1, respectively. Without loss of generality in the following we will consider, for simplicity, $n_0 = 1$. Dielectric cylinders are supposed infinitely long. They have circular cross sections with radii a_{cq} and refractive indices n_{cq} $(q = 1, ..., N)$. The cylinder axes are parallel to the interface and the wave

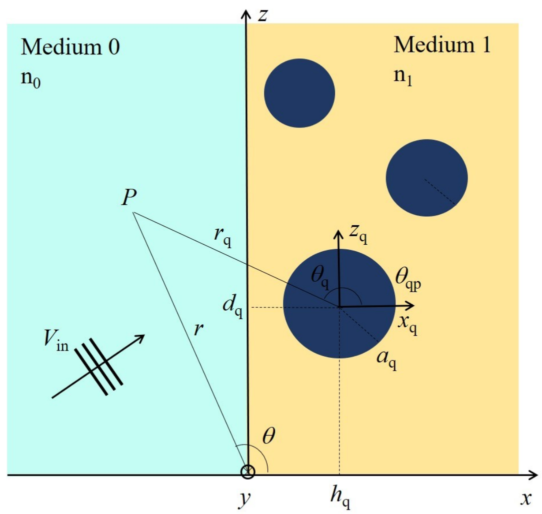

Figure 1. Geometry of the scattering problem and used coordinates.

vector of the incident plane wave is orthogonal to the cylinder axes, so that the overall problem can be considered as two-dimensional.

The scattering problem is solved in terms of the scalar function $\mathcal{V}(x, z; t)$, representing the y-directed electric field $\mathcal{E}_y(x, z; t)$ in case of TM polarization, or the y-directed magnetic field $\mathcal{H}_y(x, z; t)$, for the TE polarization.

Since the field is monochromatic with angular frequency ω, we write the field amplitude in the form

$$\mathcal{V}(x, z; t) = V(x, z) \exp(-i\omega t) \ , \tag{1}$$

and focus our attention to the space-dependent part of the plane wave, namely, $V(x, z)$. Accordingly, the expression of the incident field will be taken as

$$V_{\text{in}}(x, z) = A_{\text{in}} \exp\left[i\left(k_\perp^i x + k_\parallel^i z\right)\right] \ , \tag{2}$$

where $k_\perp^i$ and $k_\parallel^i$ are, respectively, the orthogonal and parallel components (with respect to the interface) of the wave vector $\mathbf{k}^i$ (having modulus $k_0 = 2\pi/\lambda$, with λ being the wavelength in vacuo), and A_{in} is the amplitude at $x = z = 0$. It will be also useful to introduce a set of local reference frames, RF_q ($q = 1, ..., N$), each of them centred on the qth cylinder. Both rectangular, (x_q, z_q), and polar coordinates, (r_q, θ_q), will be used. The qth cylinder has axis located in (h_q, d_q) in the main reference frame (x, z), being $x = x + h_q$ and $z = z + d_q$.

The proposed tehchnique is based on the use of suitable basis functions and takes account of all the multiple interactions among the objects, and between objects and interface. The solution is obtained by considering, in addition to the incident wave, six different contributions to the total scattered field (see Fig. 2). In particular, the field in medium 1 is expressed as the sum of three contributions, i.e.,

$$V_1 = V_{\text{t}} + V_{\text{s}} + V_{\text{sr}} \ , \tag{3}$$

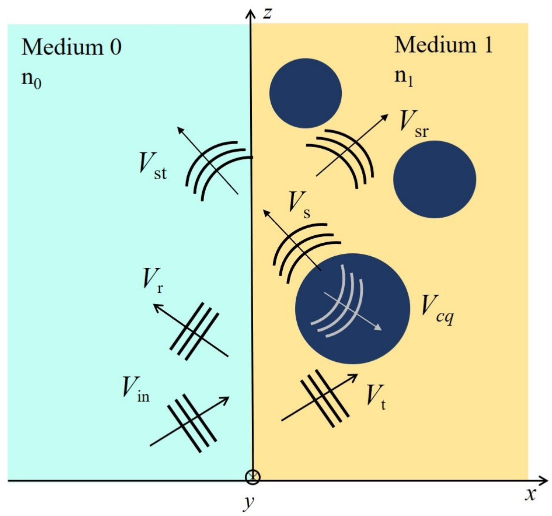

Figure 2. Different contributions to the total field.

that are, respectively:

- The field produced by the transmission of the incident plane wave through the interface:

$$V_{\mathrm{t}}(x,z) = T_{01}(k_{\|}^{i})\; A_{\mathrm{in}} \exp\left[i \left(k_{\perp}^{t} x + k_{\|}^{t} z \right) \right] \;, \tag{4}$$

where $T_{01}(k_{\|}^{i})$ is the transmission coefficient from medium 0 to medium 1 and $\mathbf{k}^{t}$ is the transmitted wave vector in medium 1, both obtained from the Fresnel formulas [38].

- The field scattered by the cylinders:

$$V_{\mathrm{s}}(x,z) = \sum_{q=1}^{N} \sum_{m=-\infty}^{+\infty} c_{qm}\, CW_{m}(k_1 x_q, k_1 z_q) \;, \tag{5}$$

expressed as the sum of the fields scattered by each cylinder, with $k_1 = n_1 k_0$ the wavenumber in Medium 1. Such fields are written as the superposition, with unknown coefficients c_{qm}, of Cylindrical Waves (CW_m) centered on the axis of each cylinder, defined as

$$CW_{m}(k_1 x_q, k_1 z_q) = H_{m}(k_1 r)\, e^{im\theta_q} \;, \tag{6}$$

with H_m being the Hankel function of the first kind and order m [39].

- The field produced by the reflection of V_{s} by the interface:

$$V_{\mathrm{sr}}(x,z) = \sum_{q=1}^{N} \sum_{m=-\infty}^{+\infty} c_{qm}\, RW_{m}\left[n_1 \left(-x_q - 2h_q \right), n_1 z_q \right] \;, \tag{7}$$

expressed in terms of Reflected Cylindrical Waves (RW_m). The latter represent the field produced by the reflection of each CW_m from the interface and are defined as [16].

$$RW_m(u,v) = \frac{1}{2\pi}\int\limits_{-\infty}^{\infty} \Gamma_{10}(k_\parallel) F_m(u,k_\parallel) e^{ik_\parallel v} dk_\parallel \ , \tag{8}$$

with $\Gamma_{10}(k_\parallel)$ being the reflection coefficient from medium 1 to medium 0, and

$$F_m(u,k_\parallel) = \frac{2}{\sqrt{k_0^2 - k_\parallel^2}} e^{i|u|\sqrt{k_0^2-k_\parallel^2}} \times \begin{cases} e^{im\arccos(k_\parallel/k_0)}, & u \geq 0 \ ; \\ e^{-im\arccos(k_\parallel/k_0)}, & u \leq 0 \ . \end{cases} \tag{9}$$

An analogous decomposition holds in medium 0, where the field is thought of as the superposition of three terms, namely,

$$V_0 = V_{\rm in} + V_{\rm r} + V_{\rm st} \ , \tag{10}$$

where, in addition to the incident wave, we have:

- The field produced by the reflection of the incident plane wave from the interface:

$$V_{\rm r}(x,z) = \Gamma_{01}(k_\parallel^i)\ A_{\rm in}\ \exp\left[i\left(-k_\perp^i x + k_\parallel^i z\right)\right] \ , \tag{11}$$

with $\Gamma_{01}(k_\parallel^i)$ being the reflection coefficient from medium 0 to medium 1.

- The field produced by the transmission of $V_{\rm s}$ through the interface:

$$V_{\rm st}(x,z) = \sum_{q=1}^{N}\sum_{m=-\infty}^{\infty} i^m c_{qm} TW_m(x - h_{\rm q}, z - d_q, h_q) \tag{12}$$

expressed in terms of Transmitted Cylindrical Waves (TW_m), representing the field produced by the transmission of each CW_m through the interface, that are defined as [16]:

$$TW_m(u,v,h) = \frac{1}{2\pi}\int\limits_{-\infty}^{\infty} T_{10}(k_\parallel) F_{\rm m}(-n_1 h, k_\parallel) e^{-i\sqrt{k_0^2-(n_1 k_\parallel)^2}(u+h)} e^{ik_\parallel v} dk_\parallel \ . \tag{13}$$

Finally, the field transmitted inside the qth cylinder is written in term of Bessel functions of the first kind, J_ℓ, with unknown expansion coefficients $d_{q\ell}$:

$$V_{{\rm c}q}(x_q,z_q) = \sum_{\ell=-\infty}^{+\infty} d_{q\ell} J_\ell(k_{{\rm c}q} r_q) e^{i\ell\theta_q} \ . \tag{14}$$

with $k_{{\rm c}q} = n_{{\rm c}q} k_0$.

Imposing the boundary conditions on the cylinders' interface and following the derivations presented in [26], the following linear system is obtained, having the coefficients $c_{\rm qm}$ as unknowns:

$$\sum_{q=1}^{N}\sum_{m=-\infty}^{+\infty} D_\ell^{qp} c_{qm} = M_\ell^p \tag{15}$$

where $D^{\mathrm{qp}}_{m\ell} = G^{p(2)}_{\ell} A^{qp(1)}_{\ell m} - G^{p(1)}_{\ell} A^{qp(2)}_{\ell m}$ and $M^{p}_{\ell} = B^{p(1)}_{\ell} G^{p(2)}_{\ell} - B^{p(2)}_{\ell} G^{p(1)}_{\ell}$, being (with $\alpha = 1, 2$)

$$
\begin{aligned}
A^{\mathrm{qp}(\alpha)}_{\ell m} = \;& i^{-\ell} T^{(\alpha)}_{\ell}(k_1 a_p) \Big\{ C W_{\mathrm{m}-\ell}(k_1 x_{\mathrm{qp}}, k_1 z_{qp})(1-\delta_{qp}) + \frac{\delta_{qp}\delta_{\ell m}}{T^{(\alpha)}_{\ell}(k_1 a_p)} \\
& + \sum_{j=1}^{+\infty} R W_{m+\ell}\left[-n_1\left(h_q + h_p\right), n_1\left(d_p - d_q\right)\right] \Big\} \qquad (16) \\
B^{\mathrm{p}(\alpha)}_{\ell} = \;& -T_{01}(k^i_{\|})\, e^{i\left[h_p \sqrt{1-(k^i_{\|}/k_1)^2} + k^i_{\|} d_p\right]}\, T^{(\alpha)}_{\ell}(k_1 a_p)
\end{aligned}
$$

where δ is the Kronecker symbol. Furthermore

$$
G^{p(1)}_{\ell} = J_{\ell}(k_{\mathrm{cp}} a_p)/H_{\ell}(k_1 a_p)\ , \qquad (17)
$$

$$
G^{p(2)}_{\ell} = g_p J'_{\ell}(k_{\mathrm{cp}} a_p)/H'_{\ell}(k_1 a_p)\ , \qquad (18)
$$

$$
T^{(1)}_{\ell}(x) = J_{\ell}(x)/H_{\ell}(x)\ , \qquad (19)
$$

$$
T^{(2)}_{\ell}(x) = J'_{\ell}(x)/H'_{\ell}(x)\ , \qquad (20)
$$

where $g_p = n_{cp}/n_1$ or n_1/n_{cp} for TM or TE polarization, respectively. The above equations allow evaluating the field everywhere outside the cylinders.

To evaluate the field inside the cylinders, the coefficients $d_{\mathrm{p}\ell}$ are needed. To this aim, we insert Eqs. (16)-(18) into Eq. (15), and after some algebra obtain

$$
\begin{aligned}
d_{p\ell} = \;& n_1 \frac{J_{\ell}(k_1 a_p) H'_{\ell}(k_1 a_p) - J'_{\ell}(k_1 a_p) H_{\ell}(k_1 a_p)}{n_1 J_{\ell}(k_1 a_{\mathrm{p}}) H'_{\ell}(k_1 a_p) - k_{\mathrm{cp}} J'_{\ell}(k_1 a_p) H_{\ell}(k_1 a_p)} \\
& \times \Bigg\{ \sum_{q=1}^{N} \sum_{m=-\infty}^{+\infty} i^{-\ell} c_{qm} \Big\{ C W_{m-\ell}(k_1 x_{qp}, k_1 z_{qp})(1-\delta_{qp}) \\
& + \sum_{j=1}^{+\infty} R W_{m+\ell}\left[-n_1\left(h_q + h_{\mathrm{p}}\right), n_1\left(d_p - d_q\right)\right] \Big\} \qquad (21) \\
& + T_{01}(k^i_{\|}) e^{i\left[h_p \sqrt{1-(k^i_{\|}/k_1)^2} + k^i_{\|} d_p\right]} \Bigg\}\ .
\end{aligned}
$$

The knowledge of the c_{qm} and d_{ℓ} coefficients gives the total electromagnetic field in any point of space and for both polarizations.

2.2. Scattering of a field nonuniform in time and space

The theory presented in Section 2.1 is generalized here to the case of a pulsed and spatially nonuniform source field. Due to the two-dimensional nature of the problem, we consider the field distribution as independent from the y-coordinate.

If the input field is not a plane wave, even in the case of free propagation, the temporal evolution of the pulse depends on the point where the field is detected, so that some care has to be put to define the temporal shape of the pulse unambiguously. In our model, we suppose that a certain plane exists in the half-space occupied by medium 0 where the field presents the same temporal behavior at any point, except for an amplitude factor. In other terms, across such plane, the time and space dependences of the field factorize. In the first part of this section, for simplicity, we will take such a plane as coincident with the planar interface between the two media. The general case will be treated later on.

Denoting by ω_0 the central frequency of the pulse, under the above hypothesis the amplitude of the incident field across the plane $x = 0$ takes the form

$$\mathcal{V}_{\rm in}(0, z; t) = B(z)\, S(t) \exp\left(-i\omega_0 t\right) \,, \tag{22}$$

where $B(z)$ gives the spatial distribution of the field across the plane and $S(t)$ the temporal envelope of the pulse.

Equation (22) can be Fourier transformed, both in time and in space, giving rise to the following expansion:

$$\mathcal{V}_{\rm in}(0, z; t) = \frac{1}{(2\pi)^2} \int_{-\infty}^{\infty} \int_{-\infty}^{\infty} b(k_\parallel)\, s(\omega - \omega_0)\, e^{i(k_\parallel z - \omega t)}\, {\rm d}\omega\, {\rm d}k_\parallel \,, \tag{23}$$

with

$$s(\omega) = \int_{-\infty}^{\infty} S(t)\, e^{i\omega t}\, {\rm d}t \,, \tag{24}$$

and

$$b(k_\parallel) = \int_{-\infty}^{\infty} B(z)\, e^{-ik_\parallel z}\, {\rm d}z \,, \tag{25}$$

expressing the incident field as a continuous superposition of monochromatic plane waves, with angular frequency ω, wave vector $(k_\parallel, k_\perp)$, being $k_\perp = \sqrt{k_0^2 - k_\parallel^2}$, and amplitude

$$A_{\rm in}(k_\parallel; \omega) = b(k_\parallel)\, s(\omega - \omega_0) \,. \tag{26}$$

The approach recalled in Sec. 2.2 can be then applied to the case of a temporally and spatially nonuniform field, by solving the scattering problem for each of the plane waves composing the incident field, and summing up the obtained solutions. In a practical application of the method, of course, time and space spectra of the input field need to be discretized and truncated, so that the scattered field will be obtained as the sum of a finite number of terms.

Now, we are able to evaluate the plane-wave spectrum of the input field for the more general case in which the plane where the time and space dependences of the field factorize [see Eq. (22)] does not coincide with $z = 0$. This model could be more appropriate when a light beam impinges onto the interface obliquely. Geometry and notations are reported in Fig. 3.

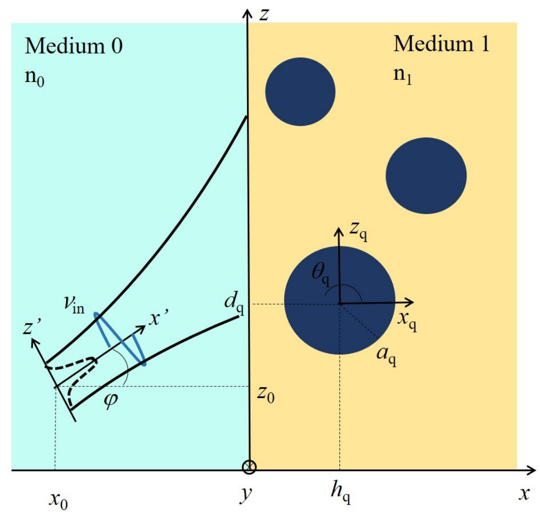

Figure 3. Geometry of the scattering problem with a pulsed beam as excitation.

In such a case, the expressions of the incident field obtained above hold in the reference frame (O', x', z'). In particular, Equation (23) reads

$$\mathcal{V}'_{\text{in}}(0, z'; t) = \frac{1}{(2\pi)^2} \int\limits_{-\infty}^{\infty} \int\limits_{-\infty}^{\infty} b'(k'_{\parallel})\, s(\omega - \omega_0)\, e^{i(k'_{\parallel} z' - \omega t)}\, \mathrm{d}\omega\, \mathrm{d}k'_{\parallel} \,, \tag{27}$$

where all primed quantities refer to the rotated reference frame. All we have to do is to write Eq. (27) in the reference frame (O, x, z), using the pertinent transformation rules, i.e.,

$$\begin{cases} z' = -x \sin\varphi + z \cos\varphi - z_0 \,, \\ x' = x \cos\varphi + z \sin\varphi - x_0 \,, \end{cases} \tag{28}$$

and

$$\begin{cases} k'_{\parallel} = -k_{\perp} \sin\varphi + k_{\parallel} \cos\varphi \,, \\ k'_{\perp} = k_{\perp} \cos\varphi + k_{\parallel} \sin\varphi \,. \end{cases} \tag{29}$$

After some analytical manipulations, the following result is obtained:

$$\begin{aligned} \mathcal{V}_{\text{in}}(0, z; t) = \; & \frac{1}{(2\pi)^2} \int\limits_{-\infty}^{\infty} \int\limits_{-\infty}^{\infty} b'(-k_{\perp} \sin\varphi + k_{\parallel} \cos\varphi)\, s(\omega - \omega_0) \\ & \times e^{-i(k_{\parallel} x_0 - k_{\perp} z_0)}\, e^{i(k_{\parallel} z - \omega t)} \left(\frac{k_{\parallel}}{k_{\perp}} \sin\varphi + \cos\varphi \right) \mathrm{d}\omega\, \mathrm{d}k_{\parallel} \,, \end{aligned} \tag{30}$$

meaning that the plane-wave spectrum of the incident field in the reference frame $(0, x, z)$ has to be taken as

$$\begin{aligned} A_{\text{in}}(k_{\parallel}; \omega) = \; & b'(-k_{\perp} \sin\varphi + k_{\parallel} \cos\varphi) \\ & \times \left(\frac{k_{\parallel}}{k_{\perp}} \sin\varphi + \cos\varphi \right) e^{-i(k_{\parallel} x_0 - k_{\perp} z_0)}\, s(\omega - \omega_0) \,. \end{aligned} \tag{31}$$

In the next Section, the presented approach will be implemented in practical numerical cases.

3. Numerical results for a pulsed Gaussian beam

The technique presented in previous Sections is applied to the case of an incident Gaussian beam. The latter propagates along the x'-axis, has waist size w_0 and center at the point (x_0, z_0). Therefore, its amplitude along the z' axis has the form

$$B'(z') = B_0\, e^{-(z'/w_0)^2}\ , \tag{32}$$

corresponding to a spatial spectrum given by:

$$b'(k'_{\parallel}) = B_0\sqrt{\pi}\, w_0\, e^{-\left(w_0 k'_{\parallel}/2\right)^2}\ . \tag{33}$$

The temporal shape of the pulse is also chosen as Gaussian, i.e.,

$$S(t) = e^{-(t/\sigma)^2}\ , \tag{34}$$

corresponding to the following frequency spectrum:

$$s(\omega) = \sqrt{\pi}\,\sigma\, e^{-(\sigma\omega/2)^2}\ . \tag{35}$$

The parameter σ represents the duration of the Gaussian pulse and can be related to the FWHM (Full Width Half Maximum) of the frequency spectrum, $\Delta\omega$, through the relation

$$\sigma = \frac{4\sqrt{\ln 2}}{\Delta\omega}\ . \tag{36}$$

The FWHM of the temporal spectrum is often expressed in terms of wavelengths $(\Delta\lambda)$ and, for narrow-band pulses with central wavelength λ_0, it is evaluated as

$$\Delta\lambda = \frac{\lambda_0^2\,\Delta\omega}{2\pi c}\ . \tag{37}$$

From Eq. (31) and the above assumptions, the amplitude of the typical monochromatic plane wave of the expansion turns out to be

$$\begin{aligned} A_{\rm in}(k_{\parallel};\omega) = \quad & B_0\pi\sigma w_0\, \exp\left[-\frac{w_0^2}{4}\left(-k_\perp \sin\varphi + k_{\parallel}\cos\varphi\right)^2\right] \\ & \times \left(\frac{k_{\parallel}}{k_\perp}\sin\varphi + \cos\varphi\right) e^{-i(k_{\parallel}x_0 - k_\perp z_0)} \\ & \times \exp\left[-\frac{\sigma^2}{4}\left(\omega-\omega_0\right)^2\right]\ . \end{aligned} \tag{38}$$

In a practical application of the method presented in Sec. 2,2, both the space and temporal spectra of the incident field will be discretized, so that the latter will be described through a suitably sized discrete and finite set of plane waves, and the involved Fourier transforms will be replaced by Fast Fourier Transforms [40].

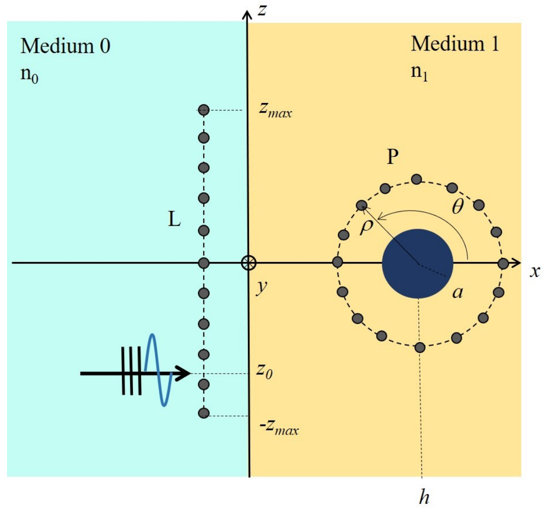

Figure 4. Geometrical layout for B-scans: polar, along a circumference surrounding the cylinder (curve P), and linear along a segment parallel to the interface (line L).

Another approximation concerns the sums required to solve the scattering problem, coming from the expansion of the involved fields in terms of cylindrical waves (see Sec. 2.1). Such sums have an infinite number of terms even for the case of single monochromatic incident plane wave. In our simulations, such sums have been truncated to the integer part of $3k_1 a_{max}$, where a_{max} is the radius of the largest cylinder, as a good compromise between accuracy and computational heaviness [41].

The method proposed in Section 2 can be applied to calculate the scattered field by a target in those applications where broadband light is used [9],[7]. The scattering problem is solved first for an incident pulsed plane wave, and this will be used as the reference case. The plane wave impinges normally ($\varphi = 0$) onto the interface and has TM polarization. A broadband light source is modelled, given by a Gaussian pulse of central wavelength $\lambda_0 = 1300$ nm, and half-bandwidth $\Delta\lambda = 400$ nm, corresponding to a pulsed duration $\sigma = 7.5 \times 10^{-3}$ ps [9].

A single scattering cylinder is considered, having radius a, refractive index $n_c = 1.5$, and axis located at a distance h from the interface. The hosting medium has refractive index $n_1 = 1.4$. In the simulations, sizes and permittivities of the cylinder are chosen to be compatible with the modelling of inclusions, such as small vessels, in biological tissues [6]-[9]. Also the small permittivity contrast between the cylindrical inclusion and the embedding medium is typical of biological systems at optical frequencies. The intensity of the scattered field is represented as a polar B-scan [9], obtained on moving the receiver point along a circle of radius ρ, centered on the cylinder axis (curve P in Fig. 4). The intensity is normalized to its maximum value and expressed in dB. Polar B-scans are reported in Fig. 5 for $\rho = 25$ μm and different values of a and h. These polar plots give an understanding of the scattering paths under plane-wave illumination. Differently from [9], where a polar bscan was evaluated for one cylinder in free space, in

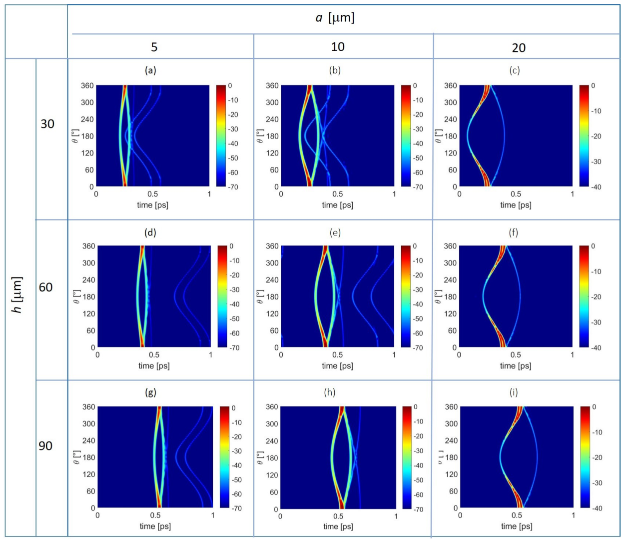

Figure 5. Polar B-scan of the normalized radiation intensity in medium 1 (in dB) along a circumference of radius $\rho = 25$ μm, as function of θ (between 0 and 360°) and time (between 0 and 1 ps). Incident plane wave with normal incidence and TM polarization. Refractive indices: $n_1 = 1.4$ and $n_c = 1.5$. Three different values of the cylinder's radius ($a = 5$, 10, 20 μm) and depths ($h = 30$, 60, 90 μm).

the following a discontinuity in the propagation media of the source field is introduced, as the source is excited in an air-filled medium, whereas the cylinder is embedded in a medium with different permittivity.

Various contributions to the total scattered field can be distinguished in the plots in Fig. 5. In order to better identify the single contributions, some A-scans, extracted from the plots of Fig. 5 (with $a = 5$ μm and $h = 30$, 60, and 90 μm), are shown in Fig. 6. The curves report the field intensity, as a function of time, revealed by a detector at a fixed position in space. In this case, such a position is at $\rho = 25$ μm and $\theta = 180°$, so that the curves correspond to the central horizontal line of the plots in the first column of Fig. 5.

In those A-scans, peaks of the radiation intensity can be identified on the basis of the delay that they present with respect to the incident pulse. Peaks are labeled with letters from A to E, with the following legend: A is the earliest pulse and corresponds to the field scattered from the front of the cylinder; B is the field scattered from its backside; C and D correspond to the reflection of the peaks A and B, respectively, from the plane interface; E comes from the surface wave travelling along the cylinder boundary, and has an arrival time very close to B. As in [9], the pulses A-B give the cylinder cross-section, as the time delay between the two peaks returns the optical distance $\Delta z = 2n_c a$, that may be evaluated also through a ray tracing approach. As to the E contribution, it can instead be calculated only through a full-wave solution of the Maxwell's equations. In Fig. 6(c), C and D are no longer visible because their arrival times are beyond the shown time window. The pulses F and G, appearing there, are the second- and third-order reflections from the interface of the field scattered from the backside of the cylinder.

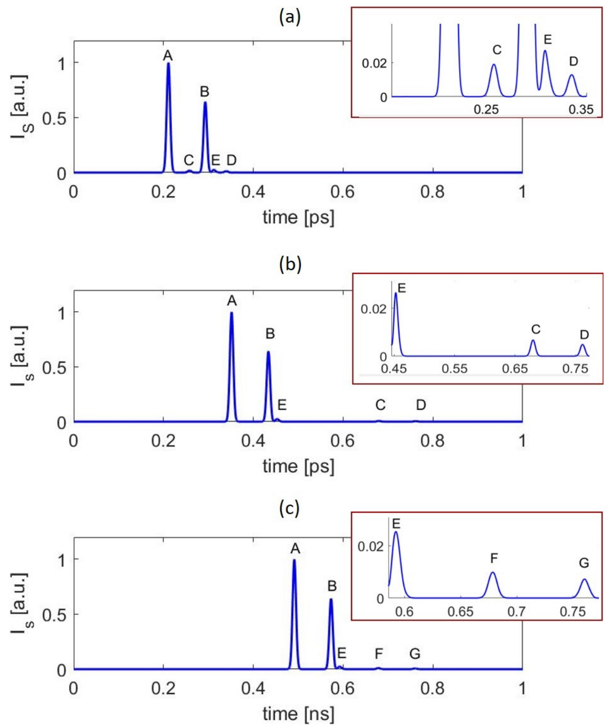

Figure 6. A-scan evaluated at $\theta = 180°$ and $\rho = 25$ μm Incident plane wave with normal incidence and TM polarization. Refractive indices: $n_1 = 1.4$ and $n_c = 1.5$. Cylinder's radius is $a = 5$ μm at three depths : a) $h = 30$ μm; b) $h = 60$ μm; c) $h = 90$ μm.

In the next example the incident field is a pulsed Gaussian beam, having TM polarization and spatial amplitude given by Eq. (32). The beam impinges normally and is focused onto the surface, so that its waist plane coincides with the surface. The temporal shape of the pulse is the same as that used in the previous example, while several values of waist size and lateral position will be considered. As for the previous example, a single scattering cylinder is present, having radius a, refractive index $n_c = 1.5$, and axis located at a distance $h = 30$ μm from the interface. Its lateral position is kept fixed ($d = 0$). The hosting medium has refractive index $n_1 = 1.4$.

B-scans of the normalized scattered intensity are reported in Figs. 7 and 8 for $a = 5$ μm and $a = 20$ μm, respectively. Such plots can be compared to the ones in Figs 5(a) and 5(c), which refer to the same choices of the parameters and an incident plane wave.

In Fig. 7, beam waist sizes are w_0 =10, 5, and 2.5 μm, while the beam is shifted from the position $z_0 = 0$ to $z_0 = 5\mu$m, and $z_0 = 10\mu$m. With the beam in the central position ($z_0 = 0$), all the plots clearly show the scattered field intensities from the top and backside of the cylinder, with a pattern analogous to the one observed with the plane-wave source (Fig. 5(a)). The reflections by the interface relevant to these two

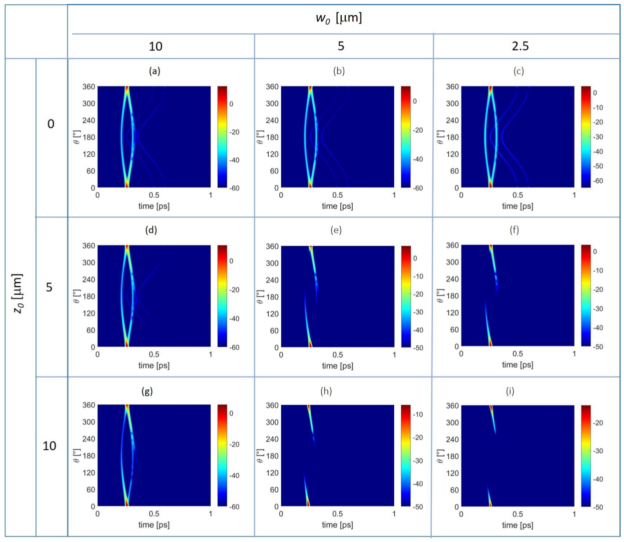

Figure 7. Polar B-scan of the radiation intensity in medium 1 (in dB) along a circumference of radius $\rho = 25$ μm surrounding the cylinder, as function of θ (between 0 and 360°) and time (between 0 and 1 ps). Impinging Gaussian beam with normal incidence and waist on the surface, in TM polarization. Refractive indices: $n_1 = 1.4$ and $n_c = 1.5$. Cylinder's radius is $a = 5$ μm and depth is $h = 30$ μm, for three values of the beam waist ($w_0 = 10$, 5, 2.5 μm) and three values of the lateral position of the waist (z_0=0, 5, 10 μm).

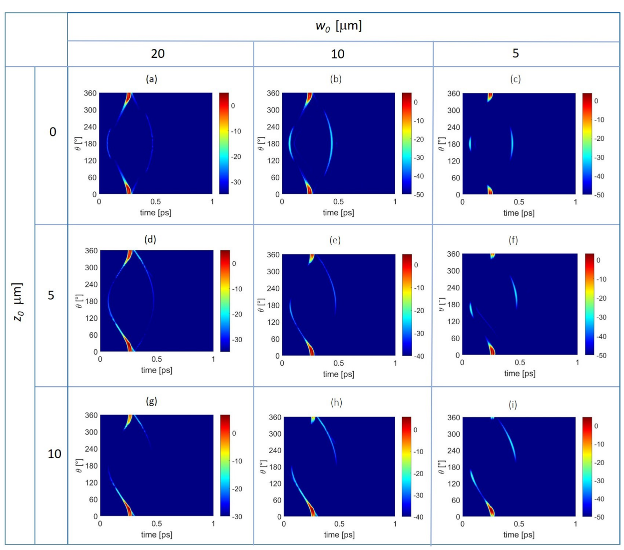

Figure 8. Polar B-scan of the radiation intensity in medium 1 (in dB) along a circumference of radius $\rho = 25$ μm surrounding the cylinder, as function of θ (between 0 and 360°) and time (between 0 and 1 ps). Impinging Gaussian beam with normal incidence and waist on the surface, in TM polarization. Refractive indices: $n_1 = 1.4$ and $n_c = 1.5$. Cylinder's radius $a = 20$ μm and depth $h = 30$ μm, for three values of the beam waist ($w_0 = 5$, 10, 20 μm) and three values of the lateral position of the waist (z_0=0, 5, 10 μm).

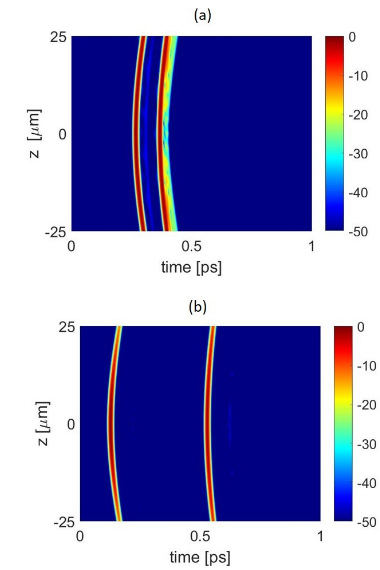

Figure 9. B-scan radargrams of the transmitted radiation-intensity for a single-cylinder layout ($h = 30$ μm, $n_1 = 1.4$, $n_c = 1.5$), incident Gaussian beam with waist in ($x_0 = 0$, $z_0 = 0$ μm), $w_0 = 5$ μm, normal incidence, TM polarization. Receivers are along a line parallel to the interface at $x = -10$ μm. a) $a = 5$ μm; b) $a = 20$ μm.

scattering contributions are also visible, especially with the smallest values of waist size, namely, $w_0 = 5\mu$m (Fig. 7(b)) and $w_0 = 2.5\mu$m (Fig. 7(c)) .

On moving the cylinder center away from the central position, radiation patterns become less and less symmetric, especially for small values of the beam spot size (second and third column of Fig. 7), but a radiation peak remains for small (and close to 360°) values of θ, corresponding to the back of the cylinder. Furthermore, on comparing the absolute values of the reported radiation intensities, it is apparent that the latter becomes negligible when the incident beam does not intercept the cylinder in a significant way (see Fig. 7(i)).

In Fig. 8, results analogous to those in Fig. 7 are reported. In this case the cylinder radius is larger ($a = 20$ μm) and the considered values of the beam waist are $w_0 = 20$, 10, and 5μm. The obtained results can be compared to the analogous ones, pertinent to the scattering of a pulsed plane wave, shown in (Fig. 5(a)).

For the same source field and geometrical layout of Figs. 7 and 8, the pattern displayed in linear B-scans are now presented. The incident beam impinges normally onto the surface, has waist size $w_0 = 5$ μm and beam center in (0,0). The scattered radiation is evaluated along a segment in medium 0, parallel to the surface, 10 μm away from it, from z $= -25$ μm to z $= 25$ μm (line L in Fig. 4). Figure 9(a) shows the linear B-scan for a cylinder with radius $a = 5$ μm, and exhibits the typical pattern relevant to targets of finite size. Two hyperbola are visibile for the scattered-transmitted radiation-intensity in medium 0: the first one is the echo of the direct scattering from the cylinder, followed by a delayed hyperbola, relevant to the intensity scattered from its backside. In Fig. 9(b), the cylinder has a larger radius ($a = 20$ μm). The two hyperbola have the same physical meaning as in the previous case but now, due to the larger size of the target, the first hyperbola is detected at earlier arrival times. The second one is delayed, due to the longer travel time through the cylinder.

4. Conclusions

In this paper, a technique for evaluating the field produced by the scattering of a pulsed light beam by a set of dielectric cylinders placed below a flat interface has been presented. Solution of the problem has been derived on an analytical basis, on extending the CWA approach to the case of fields nonuniform in space and in time. Results have been presented for both plane-wave and Gaussian-beam excitation, with Gaussian pulse temporal shape. The choice of geometrical and physical parameters show that the method can be used for simulations in biological applications.

5. Acknowledgements

The authors would like to acknowledge the Italian Ministry of Education (MIUR) for funding the Programma di Ricerca di Interesse Nazionale (PRIN) project: Ultra-wideband Virtual Imaging ExtraWall (U-View) for high-penetration high quality imagery of enclosed structures.

References

[1] S.C. Lee, C.R. Cunnigton, "Theoretical models for radiative transfer in fibrous media," *Annual Review of Heat Transfer*), C.L. Tien Ed. (Bergell House), 159-212 (1998).

[2] T. Linder, T. Löfqvist, L.G. Coppel, M. Neuman, and P, Edström, "Lateral light scattering in fibrous media," *Opt. Expr.*, **21**, 7835-7840 (2013).

[3] D. Huang, E. A. Swanson, C. P. Lin, J. S. Schuman, W. G. Stinson, W. Chang, M. R. Hee, T. Flotte, K. Gregory, C. A. Puliafito, and J. G. Fujimoto "Optical Coherence Tomography," *Science* **254**, 1178-1181 (1991).

[4] A. Knuttel et M. Boehlau-Godau, "Spatially confined and temporally resolved refractive index and scattering evaluation in human skin performed with optical coherence tomography," *J. Biomed. Opt.* **9**, 265-273 (2004).

[5] A. Knuttel, S. Bonev, and W. Knaak, "New method for evaluation of in vivo scattering and refractive index properties obtained with optical coherence tomography," *J. Biomed. Opt.* **5**, 83-92 (2000).

[6] A.E. Hartinger, A.S. Nam, I. Chico-Calero, and B.J. Vakoc, "Monte Carlo modeling of angiographic optical coherence tomography," *Biomed. Opt. Express* **5**, 4338-4349 (2014).

[7] P.R. Munro, A. Curatolo, and D.D. Sampson, "Full wave model of image formation in optical coherence tomography applicable to general samples," *Opt. Express* **23**, 2541-2556 (2015).

[8] P.R. Munro, "Three-dimensional full wave model of image formation in optical coherence tomography," *Opt. Express* **24**, 27016-27031 (2016).

[9] T. Brenner, D. Reitzle, and A. Kienle, "Optical coherence tomography images simulated with an analytical solution of Maxwell's equation for cylinder scattering," *J. Biomed. Opt.* **21**, 045001 (2016).

[10] A. Q. Howard, "The electromagnetic fields of a subterranean cylindrical inhomogeneity excited by a line source," *Geophys.* **37**, 975-984 (1972).

[11] S. O. Ogunade, "Electromagnetic response of an embedded cylinder for line current excitation," *Geophys.* **46**, 45-52 (1981).

[12] S. F. Mahmoud, S. M. Ali, and J. R. Wait, "Electromagnetic scattering from a buried cylindrical inhomogeneity inside a lossy earth," *Radio Sci.* **16**, 1285-1298 (1981).

[13] K. Hongo and A. Hamamura, "Asymptotic solutions for the scattered field of plane wave by a cylindrical obstacle buried in a dielectric half-space," *IEEE Trans. Ant. Propag.* **34**, 1306-1312 (1986).

[14] C. H. Kuo and M. Moghaddam, "Electromagnetic scattering from a buried cylinder in layered media with rough interfaces," *IEEE Trans. Antennas Propag.* **54**, 2392-2401,(2006).

[15] D. E. Lawrence and K. Sarabandi, "Electromagnetic scattering from a dielectric cylinder buried beneath a slightly rough surface," *IEEE Trans. Antennas Propag.* **50**, 1368-1376, (2002).

[16] M. Di Vico, F. Frezza, L. Pajewski, and G. Schettini, "Scattering by a finite set of perfectly conducting cylinders buried in a dielectric half-space: a spectral-domain solution," *IEEE Trans. Antennas Propag.* 53(2), 719 - 727 (2005).

[17] Y. Altuncu, A. Yapar, and I. Akduman, "On the scattering of electromagnetic waves by bodies buried in a half-space with locally rough interface," *IEEE Trans. Geosci. Remote Sensing* **44**, 6573-6592 (2006).

[18] L. Crocco, M. D'Urso, and T. Isernia, "The contrast source-extended Born model for 2D subsurface scattering problems," *Progr. Electr. Research B* **17**, 343-359 (2009).

[19] S.-C. Lee, "Scattering by closely spaced parallel nonhomogeneous cylinders in an absorbing medium," *J. Opt. Soc. Am. A* **28**, 1812-1819 (2011).

[20] S.-C. Lee, "Scattering by a radially stratified infinite cylinder buried in an absorbing half-space," *J. Opt. Soc. Am. A* **30**, 565-572 (2013).

[21] C. Bourlier, N. Pinel, and G. Kubick, Method of Moments for 2D Scattering Problems. Basic Concepts and Applications, Wiley-ISTE, 2013.

[22] C. Li, D. Lesselier, and Y. Zhong, "Full-Wave Computational Model of Electromagnetic Scattering by Arbitrarily Rotated 1-D Periodic Multilayer Structure," *IEEE Trans. Antennas Propag.* **64**, 1047 - 1060 (2016).

[23] D. J. Daniels, Surface Penetrating Radar, 2nd edition, London: IEE, 2004.

[24] C. A. Valagiannopoulos, N. L. Tsitsas, and A. H. Sihvola, "Unlocking the ground: Increasing the detectability of buried objects by depositing passive superstrates," *IEEE Trans. Geosci. Remote Sens.* **54**, 36973709 (2016).

[25] E. Porter, M. Coates, and M. Popovic, "An Early Clinical Study of Time-Domain Microwave Radar for Breast Health Monitoring," *IEEE Trans. Biomedical Eng.* **63**, 530 - 539 (2016).

[26] M. Di Vico, F. Frezza, L. Pajewski, and G. Schettini, "Scattering by buried dielectric cylindrical structures,"*Radio Science,* **40**, RS6S18 (2005).

[27] F. Frezza, L. Pajewski, C. Ponti, and G. Schettini, "Scattering by perfectly conducting circular cylinders buried in a dielectric slab through the Cylindrical Wave Approach," *IEEE Trans. Ant. Propag.*, **57**, 1208-1217 (2009).

[28] F. Frezza, L. Pajewski, C. Ponti, and G. Schettini, "Through-wall electromagnetic scattering by N conducting cylinders," *J. Opt. Soc. Am.*, **30**, 1632-1639 (2013).

[29] C. Ponti, and S. Vellucci, "Scattering by conducting cylinders below a dielectric layer with a fast non-iterative approach," *IEEE Trans. Microw. Theory Tech.*, **63**, 30-39 (2015).

[30] M.A. Fiaz, F. Frezza C. Ponti, and G. Schettini, "Electromagnetic scattering by a circular cylinder buried below a slightly rough Gaussian surface," *J. Opt. Soc. Am. A*, **31**, 26-34 (2014).

[31] C. Ponti, M. Santarsiero, and G. Schettini, "Electromagnetic Scattering of a Pulsed Signal by Conducting Cylindrical Targets Embedded in a Half-Space Medium," *IEEE Trans. Ant. Propag.*, **65**, 3073-3083 (2017).

[32] G. Cincotti, F. Gori, M. Santarsiero, F. Frezza, F. Furnò, and G. Schettini, "Plane wave expansion

of cylindrical functions," *Opt. Comm.*, **95**, 192-198 (1993).

[33] R. Borghi, F. Gori, M. Santarsiero, F. Frezza, and G. Schettini, "Plane-wave scattering by a perfectly conducting circular cylinder near a plane surface: cylindrical-wave approach," *J. Opt. Soc. Am. A*, **13**, 483-493 (1996).

[34] R. Borghi, F. Gori, M. Santarsiero, F. Frezza, and G. Schettini, "Plane-wave scattering by a set of perfectly conducting circular cylinders in the presence of a plane surface," *J. Opt. Soc. Am. A*, **13**, 2441-2452 (1996).

[35] R. Borghi, M. Santarsiero, F. Frezza, and G. Schettini, "Plane-wave scattering by a dielectric circular cylinder parallel to a general reflecting flat surface," *J. Opt. Soc. Am. A*, **14**, 15001504 (1997).

[36] S.L. Jacques and S.A. Prahl"Modeling optical and thermal distributions in tissue during laser irradiation," *Lasers in Surg. Med.* **6**, 494-503 (1987).

[37] T.K. Biswas and T.M. Luu,"In vivo MR measurement of refractive index, relative water content and T2 relaxation time of various brain lesions with clinical application to discriminate brain lesions," *Internat. J. Radiol.* **13** (2011).

[38] M. Born, and E. Wolfe, Principles of Optics, 7th edition, Cambridge University Press, 1999.

[39] C.A. Balanis, Advanced Engineering Electromagnetics, 2nd edition, Wiley, 2012.

[40] E.O. Brigham, The Fast Fourier Transform and Its Applications, Prentice Hall, USA, 1988.

[41] A. Z. Elsherbeni, "A comparative study of two-dimensional multiple scattering techniques," *Radio Sci.*, **29**, 1023-1033 (1994).